# Vertical Multi-Junction Laser Power Converters with 61% Efficiency at 30 W Output Power and with Tolerance to Beam Non-Uniformity, Partial Illumination, and Beam Displacement

**Simon Fafard \* and Denis Masson**

Broadcom (Canada), IFPD, Ottawa, ON K1A 0R6, Canada; denis.masson@broadcom.com
\* Correspondence: simon.fafard@broadcom.com

**Abstract:** Stable and reliable optical power converting devices are obtained using vertical multi-junction laser power converters. They are based on the GaAs and the InP material systems and are used for power-over-fiber or power-beaming applications. This study demonstrates that, in addition to providing the overall best conversion efficiencies with output voltages ideal for various applications, these semiconductor photovoltaic devices are very tolerant to beam non-uniformity, partial illumination, or beam displacement variations. Examples are given with two tight beams, each covering as little as ~7% of the cell area. An optical input power of 10 W was converted with still an efficiency of Eff ~59.4%. For an input power of 20 W, the illuminated area was set to ~22% without significantly affecting the conversion efficiency of Eff ~60%. Remarkably, for a beam diameter at ~65% of the chip length (i.e., covering ~35% of the chip area), a converted power of 29.5 W was obtained using a 12-junction GaAs device with a conversion efficiency of 61%. For a 10 junction InP-based device, an efficiency of Eff = 51.1% was obtained at an output voltage reaching as high as $V_{oc} = 5.954$ V for an average optical intensity of 69 W/cm$^2$ and an illumination area of ~57%.

**Keywords:** optical power converters; laser power converters; power-over-fiber; power beaming; photovoltaic; galvanic isolation; GaAs; InGaAs; InP; multi-junction semiconductor heterostructures; photonic power converters

## 1. Introduction

Laser Power Converters (LPCs) or Optical Power Converters (OPCs) [1–52] are now available for various wavelength ranges for applications with different output power requirements [37] and for cryogenic applications [46]. The ongoing developments in the field of photovoltaic (PV) devices are expected to result in further device improvements [53–88]. Such advances allow emerging applications of optical wireless power transmission (OWPT) and enable new system design strategies [89–101]. Importantly, it has become evident in recent years that vertical multi-junction OPCs are by far the best option for obtaining high output powers and high conversion efficiencies [41,91].

In addition, it is very typical for the laser beam impinging on OPC chips to have non-uniform illumination characteristics. This is a particularity of actual OWPT and power-over-fiber (PoF) applications. For example, the perimeter area of the chip is usually not illuminated to avoid the spilling (wasting) of the input power outside the active chip area. Consequently, the chip is only partially illuminated, and sometimes the beam can be displaced away from a central alignment. Moreover, the laser beam itself does not offer a uniform illumination characteristic. It typically has a peaky shape in the center of the laser spot and/or some hot spots within the beam profile.

In this study, we verify, in further detail, the performance characteristics of vertical multi-junction OPCs under non-uniform illumination conditions. We study high-power OPCs with 12 thin GaAs subcells (PT12) at up to ~50 W of non-uniform input power with an input wavelength of ~808 nm. The results with one non-uniform beam or two tight

non-overlapping beams reveal that the GaAs PT12 based on the multi-junction Vertical Epitaxial Heterostructure Architecture (VEHSA) design [70] is highly tolerant to beam non-uniformity, partial illumination, and beam displacements. Similar results are obtained for the long-wavelength InP-based OPCs, using an InGaAs/InP PT10 design with an input illumination near 1470 nm.

## 2. Materials and Methods

The GaAs PT12 is based on the previously described VEHSA design [70,71]. The Beer–Lambert law is used to determine the thicknesses of the individual GaAs subcells, with each subcell absorbing ~1/12 of the incident light. To realize the required photocurrent matching condition, the subcells have increasing thicknesses from the top subcell (thinnest) toward the bottom subcell (thickest). A total absorber thickness of 4500 nm was used for the sum of all subcells. The methodology for implementing the Beer–Lambert approach has been described previously [70,71]. In this study, no corrections have been introduced for photon coupling and recycling effects. It is known that vertical multi-junction devices can benefit from photon coupling and recycling within and between the constituent subcells [84–87]. However, such effects have more impact on the performance of the operation away from the peak of the spectral response [85]. In this study, the OPCs are operated near the peak of their spectral response, and no corrections of the subcell's thicknesses were therefore employed compared to the nominal Beer–Lambert approach.

The epitaxial layers are grown using the commercial production of Aixtron Metal Organic Chemical Vapor Deposition (MOCVD) reactors. Manufacturing microfabrication processes are used to transform the PT12 epitaxial wafers into 10 mm × 10 mm chips with connecting busbars at the two opposite sides of the chips. The devices include standard blanket back-metallization, front ohmic contacts, and antireflection coatings (ARCs). The ARC is constructed from layers of $Al_2O_3$ and $TiO_2$ and typically reduces the reflectivity (R) of the incident beam to R < 4% for the spectral range of interest.

The chips are assembled into chip-on-carrier (CoC) units. A manufacturing soldering process onto AlN carriers was used to obtain low thermal resistivity. The CoC pictures are also shown in the figures below. The same approach was applied for the long-wavelength InP-based OPCs but using a PT10 design with 10 thin InGaAs absorbers grown on the InP [45]. The CoCs are mounted onto a commercial aluminum heatsink with a high-conductivity thermal interface material (TIM) to ensure efficient heat dissipation. Low-resistance gauge AWG14 wires extracted the electrical output power from the mounted CoCs. The current–voltage (I–V) characteristics were acquired with Keithley 2601B and 2461 source meters. For the I–V measurements, the tip of the fiber-coupled laser was positioned in front of the CoC at near-normal incidence. The distance between the fiber tip and the CoC was adjusted to obtain the desired spot size from the diverging beam. The laser had an NA of ~0.22. For the experiments employing two laser beams, the tips from two fibered lasers were positioned in front of the sample. Both lasers were at near-normal incidence with respect to the sample. The lasers operated in a continuous (CW) mode. Quick I–V scans were used to minimize any chip heating or temperature drifts between the measurements.

## 3. Results

A typical cross-section of the laser beam profile is shown in Figure 1. The beam exiting the fiber tip of a multimode fibered 808 nm laser diode was projected onto a screen (top of Figure 1).

In this example, the fiber has a core of 0.105 mm and a numerical aperture of NA ~ 0.22. The image, taken at 50 cm from the fiber tip, was digitized to evaluate the intensity profile (bottom of Figure 1). The vertical scale is in arbitrary units and proportional to the laser power, whereas the horizontal scale is proportional to the spatial dimension along a central cut of the laser spot. Typically, the (x,y) centerline profile can be fitted with a super-Gaussian line shape of the type $y = A \, exp \, [2(x - c)/w)]^4 + b$, with A being proportional to the beam

power, c as the beam center position, was a measure of the beam width, and b as a constant matching the baseline background illumination of the image. Clearly, the beam intensity is non-uniform, having a maximum near the center and speckles arising from multi-mode interference.
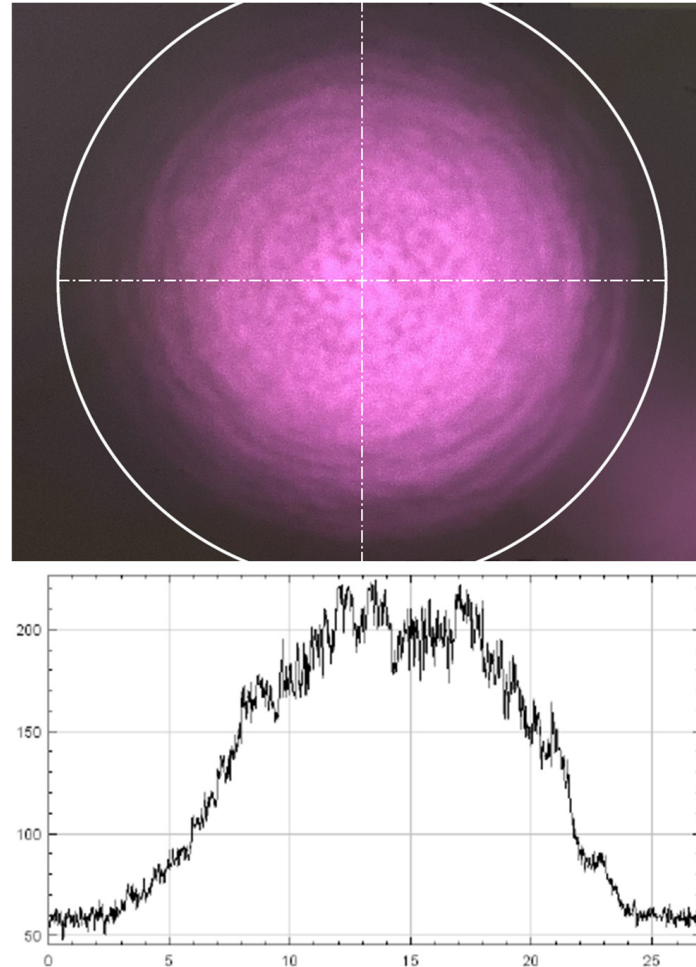


**Figure 1.** Typical beam profile exiting the fiber tip of a fibered 808 nm laser diode. Vertical scale (arb. units) is proportional to the laser power. Horizontal scale (arb. units) is the spatial dimension along a central cut of the laser spot.

The GaAs-PT12 characteristics at 20 °C are shown in Figure 2 for the typical super-Gaussian illumination described above. The measured I-V curves are shown for various optical input powers between $P_{in}$ = 5 W and $P_{in}$ = 48.2 W at a laser wavelength of ~810 nm. The beam diameter is estimated here at ~65% of the chip's side length, therefore covering ~35% of the chip area. Remarkably, a converted power of 29.5 W is obtained with a conversion efficiency of 61%.

This key new result, measured with the PT12 of Figure 2, is added as a data point (52) in Figure 3. This updated power converter performance chart is built from the results published in the literature [41,45].

In Figure 2, the I–V curves for the six lowest powers were obtained with a single high-power laser, while the I–V curves for the three highest powers were obtained with two lasers. In the latter case, the individual high-power lasers had overlapping spots of similar size, referred to as the dual beam approach. Evidently, high conversion efficiencies are obtained using the PT12 at high input powers. Such a good performance is measured despite the non-uniform super-Gaussian illumination and a large degree of partial (under-filled) illumination.
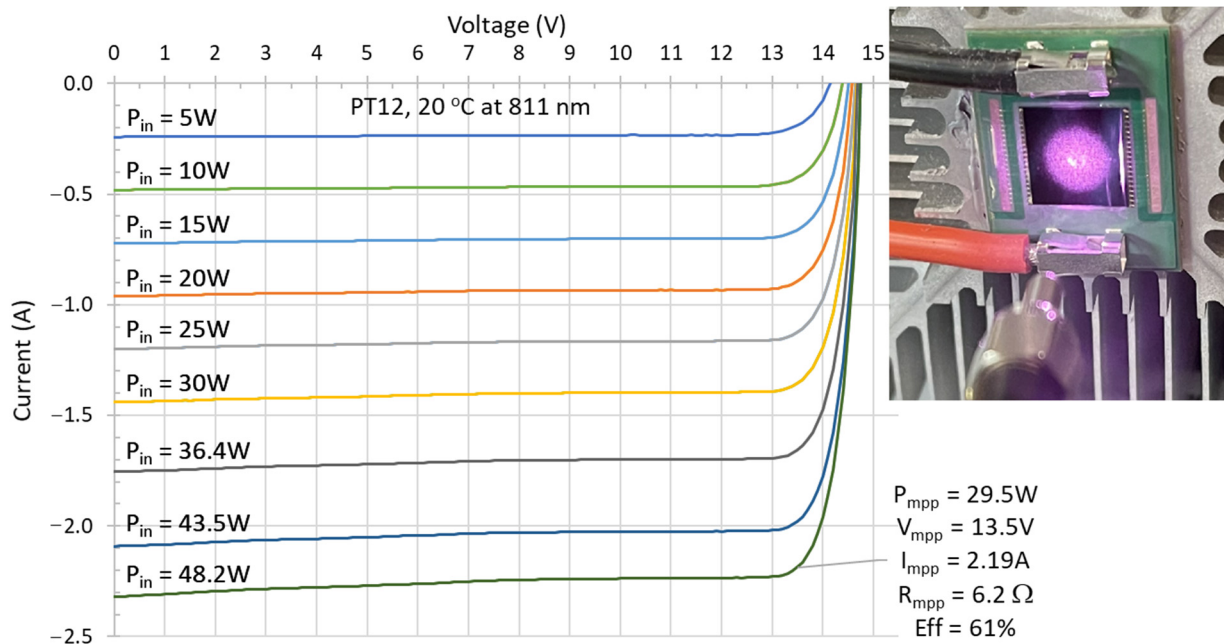
**Figure 2.** Current–Voltage curves for 10 mm × 10 mm *High-Power* multi-junction PT12. The input power ($P_{in}$) is indicated. Picture of the sample, as illuminated with a fibered high-power laser at ~811 nm, is on the right. The fiber tip is also captured in the image at the bottom center of the picture.
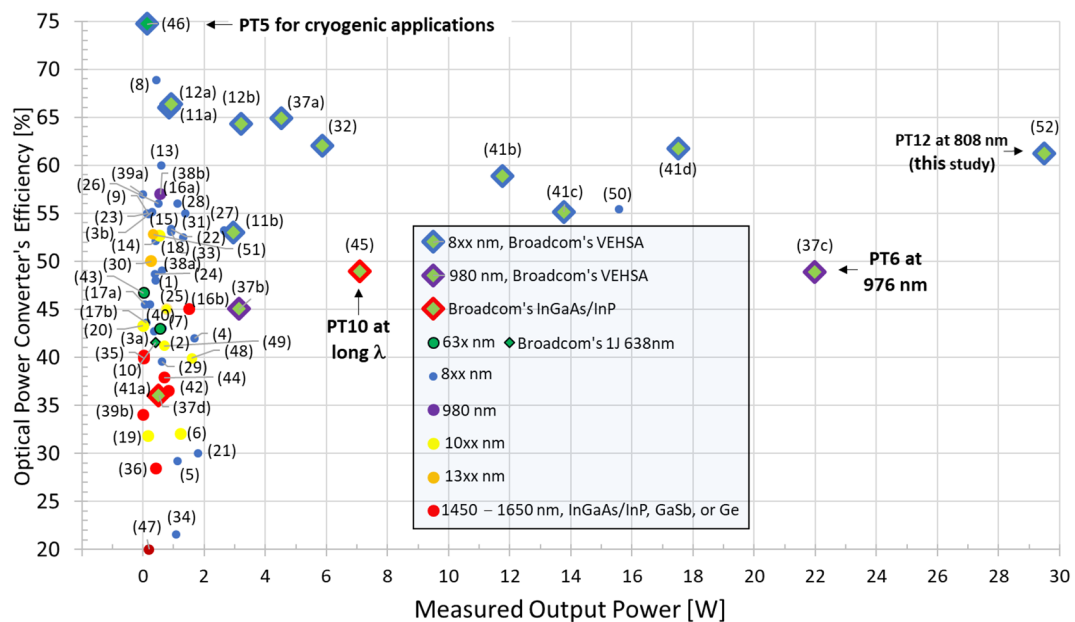


**Figure 3.** Updated Power Converter Performance Chart [41,45], including PT12 results of this study shown with data point (52). Broadcom's vertical multi-junction data are shown with diamond-shaped symbols. Details for data points (1) to (44) are found in reference [45] or from the references herein with the matching numbers in the reference section. The descriptions for the new data points are as follow: (45) PT10 InGaAs/InP [45], (46) cryogenic PT5 [46], (47) Ge cells [47], (48) metamorphic 1J 1064 nm [48], (49) 6J 1064 nm [49], (50) 6J 808 nm [50], (51) 1J InGaAsP [51], and (52) GaAs PT12 in this study. Updated from Fafard, S. and Masson, D.P., Photonics 9, 438 (2022). Copyright 2022 Author(s), licensed under a Creative Commons Attribution (CC BY) license [45].

Further below, dual-beam and tight-beam approaches are used to further investigate the impact of the beam non-uniformity, partial illumination, and beam displacement on the

performance of vertical multi-junction OPCs. The obvious advantage of using an under-filled illumination on the PV chips is to minimize the loss of the incident light. For larger spots, the fringe of the laser spatial power distribution might be falling outside the chip active area. Using an under-filled illumination also reduces alignment tolerance constraints in practical systems. For these reasons, all the results presented here are obtained with various degrees of under-filled illumination. Similarly, in field operation, the OPCs are typically operated in under-filled mode. The drawbacks of partial illumination are a slight reduction in the output voltage due to the additional dark currents from the un-illuminated chip area, a concentration of the heat profile on a smaller area of the chip, and additional semiconductor material consumption. From an economic perspective, it can be advantageous to use as much of the chip area as possible to reduce wafer usage. Nevertheless, at high illumination intensities (i.e., photocurrent much greater than dark current) on an assembly with minimal thermal resistance, the results of this study demonstrate that the vertical multi-junction OPCs are providing high-performance under partial illumination.

Another key attribute of multi-junction OPCs is that the structure uniquely allows efficient high-power conversion due to its higher optimal load. By design, the maximum power of a multi-junction device occurs at a higher operating voltage and proportionally lower operating currents. This is best shown by updating the optimal load vs. the output power chart for different OPC designs at various wavelengths of operation [45]. Figure 4 shows the chart updated with the PT12-GaAs dual-beam results from this study. The new results (green circles) match and extend those previously obtained at lower powers (green Xs). The PT12 is still maintaining an optimal load $R_{mpp}$ above 6 ohms for an output power of $P_{mpp}$ ~30 W.



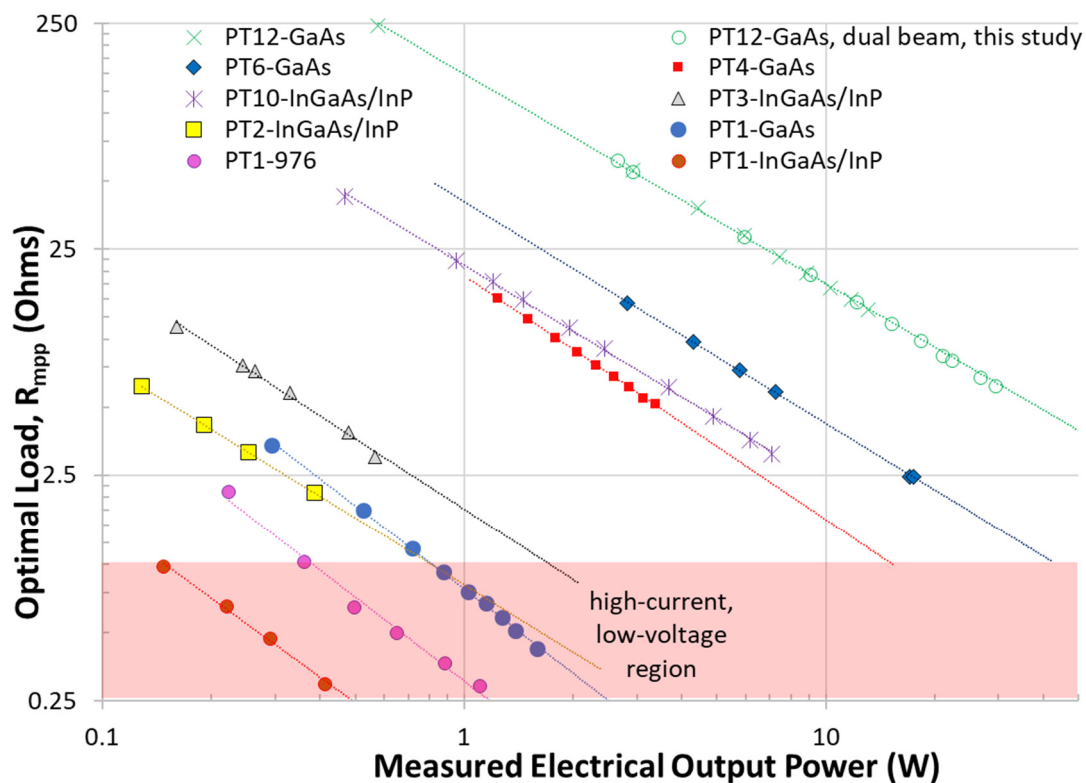**Figure 4.** Multi-junction OPCs allow efficient high-power conversion for various wavelengths of operation [45]. Chart updated with PT12-GaAs dual-beam results from this study (green circles). Lines are linear corresponding regressions. Updated from Fafard, S. and Masson, D.P., Photonics 9, 438 (2022). Copyright 2022 Author(s), licensed under a Creative Commons Attribution (CC BY) license [45].

For single-junction OPCs, the unavoidable and detrimental consequences of operating at high currents and relatively low voltages are that the optimal-load $R_{mpp}$ is eventually collapsing to unpractically small values (a few hundred milliohms). Larger optimal loads are necessary to avoid high output currents and the associated resistive losses. Losses from external parasitic resistances, such as wiring, gridline, and sheet-conduction resistances, can become significant when the optimal load becomes of comparable value [41].

Here, two methods were used to further investigate the tolerance of vertical multi-junction OPCs to beam non-uniformity, partial illumination, and beam displacements. The results are shown in Figure 5 for the GaAs-PT12 structure. The upper part of Figure 5 shows the I–V curves obtained with a single beam of ~20 W at 811 nm, covering different ratios of the chip's active area. For curve (1) and picture (1), the estimated illumination fraction is ~64%. For curve (2) and picture (2), the illuminated fraction is reduced to ~33%. For curve (3) and picture (3), it is further reduced to ~22%. Within +/−10 mV, all three cases result in a very similar open circuit voltage, $V_{oc}$ = 14.62 V. Similarly, the entire I–V curves for the tight-beam cases 2 and 3 are not really distinguishable with a $P_{mpp}$ = 12.3 W of output power converted at an efficiency of 60.5%. The larger beam of case 1 also produced very similar I–V characteristics, except for a lower photocurrent by about 1.2%. The photocurrent reduction is presumably caused by a tiny fraction of the laser spot impinging outside the active area of the chip.

The lower part of Figure 5 shows the I–V curves obtained with a dual-beam approach, each carrying 5 W of input power. For a dual narrow-beam case (bottom left picture), each beam has an estimated illumination fraction of only ~7%; they are non-overlapping and displaced away from the central area of the chip. This is contrasted with a dual-broad beam (bottom right picture), in which case each beam has an estimated illumination fraction of ~39%; they are centered on the chip and overlapping. Within the measurement uncertainties, the entire I–V curves for both cases are not distinguishable with $P_{mpp}$ = 5.9 W of output power converted with an efficiency of 59.4%.

A similar situation was observed for the long-wavelength InGaAs/InP OPCs below. These were also found to have comparable robustness to beam non-uniformity, partial illumination, or beam displacement variations [45]. The results for an InP-based 10-junction InGaAs device (PT10 InGaAs/InP) are shown in Figure 6. The I–V curves obtained at 1466 nm are in Figure 6a for a *regular-power* chip having an active area of 0.029 cm$^2$. The highest efficiency was obtained at an input power of 1.5 W, peaking here at Eff = 51.7%. New record performances are obtained, achieving an efficiency of Eff = 51.1% with an output power of up to $P_{mpp}$ = 1.02 W. At 2 W of input power, the average optical intensity is 69 W/cm$^2$, the optimal load is $R_{mpp}$ = 25.5 Ohms, and the output voltage reaches as high as $V_{oc}$ = 5.954 V. A detailed analysis of the I–V curves reveals that the output voltage follows the expected logarithmic progression of a PV diode with a correlation factor of $R^2$ = 0.98 up to 2 W of input power. The output current increases linearly with a correlation factor of $R^2$ = 0.9998 with a slope of 106.4 mA/W for $I_{sc}$ and 100.6 mA/W for $I_{mpp}$. This corresponds to external quantum efficiencies of $EQE_{sc}$ = 90.0% and $EQE_{mpp}$ = 85.1% for the EQE at the short-circuit current and maximum power points, respectively.

As is typically the case, the results of Figure 6a were obtained in under-filling illumination mode: the distance between the tip of the fibered laser and the sample was of 3 mm, giving an estimated chip illumination coverage of ~57% based on the divergence characteristics of the laser. We were not able to obtain images in this case due to the tight geometry and lack of camera sensitivity at longer wavelengths. Nevertheless, the tip distance could be varied to verify the performance as a function of the spot size on the active area of the chip.

The measurements of the PV performance with varied chip illumination coverage are shown in Figure 6b, clearly showing high robustness to the laser beam under-filling of the active area. The estimated chip illumination coverage is varied between ~23% and ~88% (tip distances between 1.5 mm and 4 mm, respectively). Meanwhile, the measured variations in the efficiency and $V_{oc}$ are minimal, with a relative variation of 1.8% and 0.7%,

respectively. The maximum efficiency is obtained at 3 mm. With larger separations, a slight decrease is observed, presumably caused by spillage outside the active area of the beam's fringe light. As expected, the $V_{oc}$ is lowest at the closest separation at 1.5 mm with $V_{oc}$ = 5.884 V but only 39 mV lower than at 4 mm of separation.
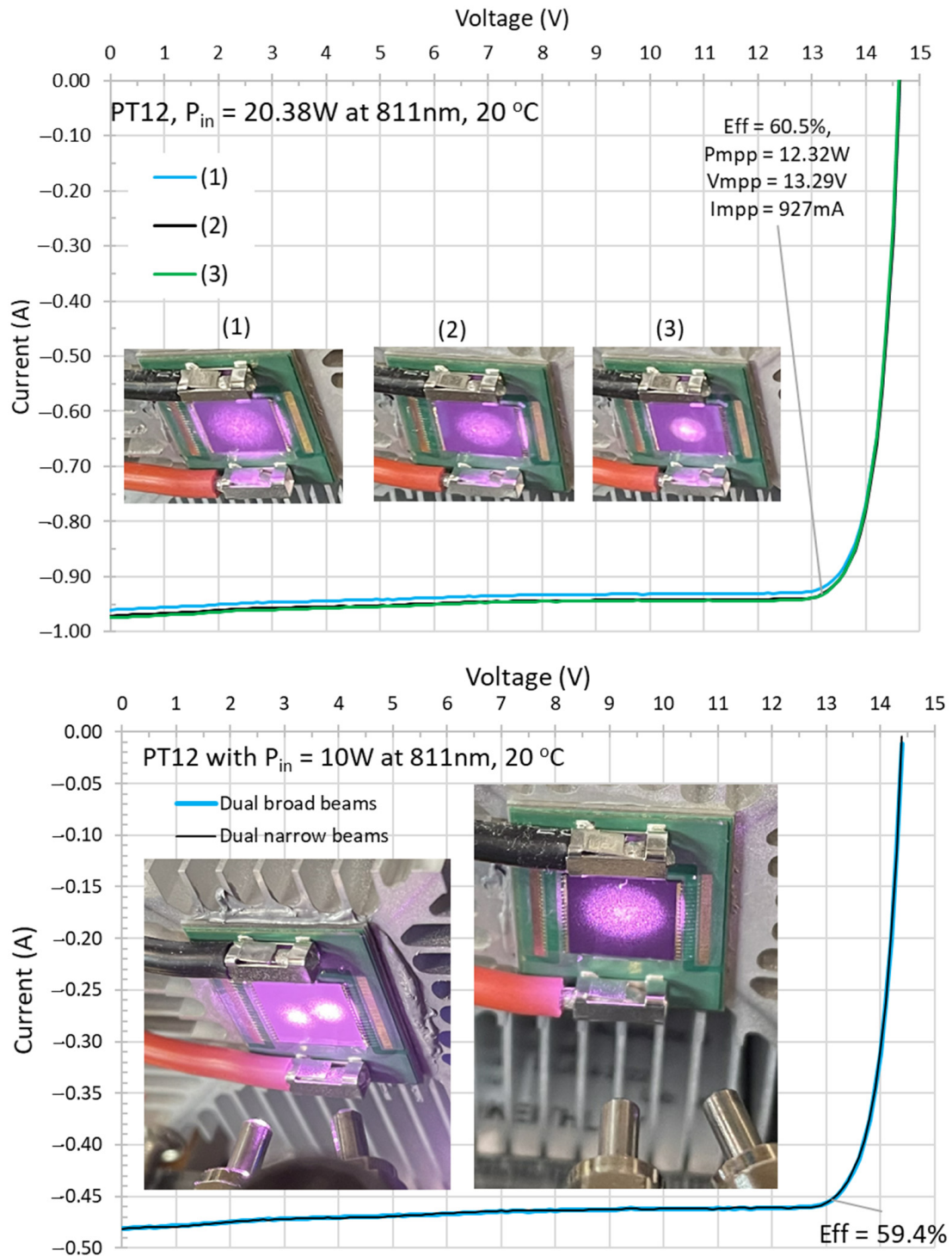


**Figure 5.** Measurement of the robustness of the 10 mm × 10 mm OPCs to beam non-uniformity and displacement. The top is for the case of under-filling of the chip (partial illumination), bottom is for the case of two displaced tight beams vs. two coincidentally larger beams. The fiber tips are also captured at the bottom center of each image for the bottom pictures.
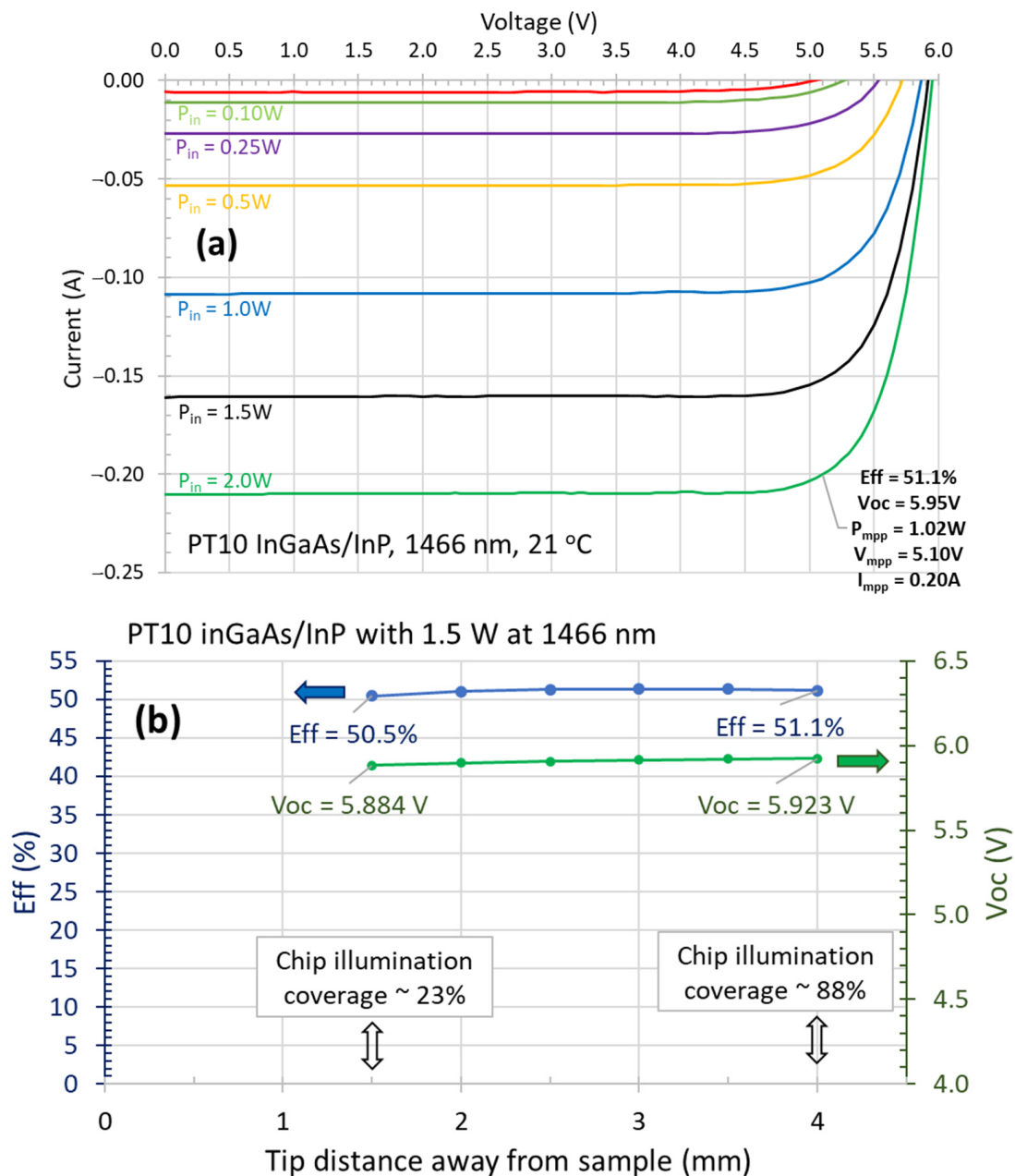
**Figure 6.** Long-wavelength OPC results at 21 °C at 1466 nm. I–V curves of a PT10 InGaAs/InP with an active area of 0.029 cm$^2$, giving efficiencies up to Eff = 51.1% with an output power of up to 1.02 W in (**a**) measurement of the performance with varied chip illumination coverage and (**b**) showing high robustness to illumination under-filling of the active area.

## 4. Discussion

For most applications, it is advantageous to operate the laser power converter devices in an under-filled illumination mode to avoid wasting the beam's fringe power, which can reach outside the chip's active area if the spot size is too large or misaligned. Indeed, working with a smaller spot size relative to the chip size also allows more tolerance to the variations in the beam alignment. However, it is normally advantageous in production to minimize as much of the chip area as possible to reduce the cost per chip.

In any case, the laser beam typically has a round geometry and a peaky profile, whereas the chip geometry is normally square. Under these conditions, partial illumination is unavoidable unless beam-shaping strategies are used. The upper limits on how much

power can be delivered on a tight spot are expected to be determined from thermal and potentially optical-intensity considerations. For example, a voltage drop will be observed if the local optical intensity generates photocurrents exceeding the peak current capabilities of the tunnel junctions. From a thermal perspective, high-enough spatially concentrated currents can lead to sudden run-away conditions. The latter can cause localized thermal stresses that can damage the chip, including cracking or local burning. Good thermal conduction in the chip assembly process is, therefore, critical to avoid chip damage under a concentrated beam operation.

## 5. Conclusions

We used two incident tight beams to verify the performance changes with the illumination ratio of the active area of the chip. We demonstrated that, for the extreme cases when the beams are covering only about 7% or less of the cell area, the GaAs-based PT12 OPC can still convert 10 W of the optical input power with an efficiency of Eff ~59.4%. For an input power of 20 W, the illuminated area has been reduced to ~22% without significantly affecting the conversion efficiency of Eff ~60%. For a larger beam diameter at ~65% of the chip side length (i.e., covering ~35% of the chip area), a converted power of 29.5 W was obtained using a 12-junction GaAs device with a conversion efficiency of 61%. The 12-junction design allowed us to maintain an optimal load $R_{mpp}$ of above 6 ohms for an output power of $P_{mpp}$ ~30 W.

The long wavelength PT10 InGaAs/InP OPCs were also found to have comparable robustness to beam non-uniformity, partial illumination, or beam displacement variations. Top performances were obtained for laser power converters in that spectral range. These PT10 InGaAs/InP achieved an efficiency of Eff = 51.1% with an output power of up to $P_{mpp}$ = 1.02 W. Their output voltage reached as high as $V_{oc}$ = 5.954 V for an average optical intensity of 69 W/cm$^2$. The measured variations in the efficiency and $V_{oc}$ were found to be minimal, a relative 1.8% and 0.7%, respectively, while the chip illumination coverage varied between ~23% and ~88%.

We found that the relatively larger spot size still leads to the highest performance, as expected, but the efficiency and output voltage penalties for using a smaller and peaky beam are relatively minor. The main considerations in using smaller non-uniform beams are rather related to the eventual limitations in the maximum input power that could arise due to concentrated thermal profiles under these conditions.

In conclusion, record efficiencies and output powers have been established for operation at ~808 nm and ~1470 nm. Our experimental results also demonstrated that, in addition to providing the overall best conversion efficiencies, with output voltages ideal for various applications, the GaAs-based and InP-based multi-junction photovoltaic devices are very tolerant to beam non-uniformity, partial illumination, or beam displacement variations.

**Author Contributions:** Conceptualization, S.F. and D.M.; methodology, S.F. and D.M.; software, S.F. and D.M.; validation, S.F. and D.M.; formal analysis, S.F. and D.M.; investigation, S.F. and D.M.; data curation, S.F. and D.M.; writing—original draft preparation S.F.; writing—review and editing S.F. and D.M.; visualization, S.F.; project administration, S.F. and D.M.; funding acquisition, S.F. and D.M. All authors have read and agreed to the published version of the manuscript.

**Institutional Review Board Statement:** Not applicable.

**Informed Consent Statement:** Not applicable.

**Data Availability Statement:** The data that support the findings of this study are available from the corresponding author upon reasonable request.

**Conflicts of Interest:** The authors declare no conflict of interest, but it should be noted that the authors are employed by Broadcom, a company that manufactures and sells semiconductor components, including power converter devices.

# References

1. Jomen, R.; Tanaka, F.; Akiba, T.; Ikeda, M.; Kiryu, K.; Matsushita, M.; Maenaka, H.; Dai, P.; Lu, S.; Uchida, S. Conversion efficiencies of single-junction III–V solar cells based on InGaP, GaAs, InGaAsP, and InGaAs for laser wireless power transmission. *Jpn. J. Appl. Phys.* **2018**, *57*, 08RD12. [CrossRef]
2. Komuro, Y.; Honda, S.; Kurooka, K.; Warigaya, R.; Tanaka, F.; Uchida, S. A 43.0% efficient GaInP photonic power converter with a distributed Bragg reflector under high-power 638 nm laser irradiation of 17 Wcm$^{-2}$. *Appl. Phys. Express* **2021**, *14*, 052002. [CrossRef]
3. Schubert, J.; Oliva, E.; Dimroth, F.; Guter, W.; Loeckenhoff, R.; Bett, A.W. High-Voltage GaAs Photovoltaic Laser Power Converters. *IEEE Trans. Electron Devices* **2009**, *56*, 170–175. [CrossRef]
4. Zhao, Y.; Sun, Y.; He, Y.; Yu, S.; Dong, J. Design and fabrication of six-volt vertically-stacked GaAs photovoltaic power converter. *Sci. Rep.* **2016**, *6*, 38044. [CrossRef] [PubMed]
5. Sun, Y.-R.; Dong, J.-R.; He, Y.; Zhao, Y.-M.; Yu, S.-Z.; Xue, J.-P.; Xue, C.; Wang, J.; Lu, Y.-Q.; Ding, Y.-W. A six-junction GaAs laser power converter with different sizes of active aperture. *Optoelectron. Lett.* **2017**, *13*, 21–24. [CrossRef]
6. Yin, J.; Sun, Y.; Yu, S.; Zhao, Y.; Li, R.; Dong, J. 1064 nm InGaAsP multi-junction laser power converters. *J. Semicond.* **2020**, *41*, 062303. [CrossRef]
7. Huang, J.; Sun, Y.; Zhao, Y.; Yu, S.; Dong, J.; Xue, J.; Xue, C.; Wang, J.; Lu, Y.; Ding, Y. Four-junction AlGaAs/GaAs laser power converter. *J. Semicond.* **2018**, *39*, 044003. [CrossRef]
8. Helmers, H.; Lopez, E.; Höhn, O.; Lackner, D.; Schön, J.; Schauerte, M.; Schachtner, M.; Dimroth, F.; Bett, A.W. 68.9% Efficient GaAs-Based Photonic Power Conversion Enabled by Photon Recycling and Optical Resonance. *Phys. Status Solidi (RRL) Rapid Res. Lett.* **2021**, *15*, 2100113. [CrossRef]
9. Oliva, E.; Dimroth, F.; Bett, A.W. GaAs converters for high power densities of laser illumination. *Prog. Photovolt. Res. Appl.* **2008**, *16*, 289–295. [CrossRef]
10. Mukherjee, J.; Jarvis, S.; Perren, M.; Sweeney, S.J. Efficiency limits of laser power converters for optical power transfer applications. *J. Phys. D Appl. Phys.* **2013**, *46*, 264006. [CrossRef]
11. Fafard, S.; York, M.C.A.; Proulx, F.; Valdivia, C.E.; Wilkins, M.M.; Arès, R.; Aimez, V.; Hinzer, K.; Masson, D.P. Ultrahigh efficiencies in vertical epitaxial heterostructure architectures. *Appl. Phys. Lett.* **2016**, *108*, 071101. [CrossRef]
12. Fafard, S.; Proulx, F.; York, M.C.A.; Richard, L.S.; Provost, P.O.; Arès, R.; Aimez, V.; Masson, D.P. High-photovoltage GaAs vertical epitaxial monolithic heterostructures with 20 thin p/n junctions and a conversion efficiency of 60%. *Appl. Phys. Lett.* **2016**, *109*, 131107. [CrossRef]
13. Khvostikov, V.P.; Kalyuzhnyy, N.A.; Mintairov, S.A.; Sorokina, S.V.; Potapovich, N.S.; Emelyanov, V.M.; Timoshina, N.K.; Andreev, V.M. Photovoltaic laser-power converter based on AlGaAs/GaAs heterostructures. *Semiconductors* **2016**, *50*, 1220–1224. [CrossRef]
14. Olsen, L.C.; Huber, D.A.; Dunham, G.; Addis, F.W. High efficiency monochromatic GaAs solar cells. In Proceedings of the Conference Record of the Twenty-Second IEEE Photovoltaic Specialists Conference—1991, Las Vegas, NV, USA, 7–11 October 1991; pp. 419–424.
15. Krut, U.D.; Sudharsanan, R.; Isshiki, T.; King, R.; Karam, N.H. A 53% high efficiency GaAs vertically integrated multi-junction laser power converter. In Proceedings of the 65th DRC Device Research Conference, South Bend, IN, USA, 18–20 June 2007; art. no. 4373680. pp. 123–124.
16. Andreev, V.; Khvostikov, V.; Kalinovsky, V.; Lantratov, V.; Grilikhes, V.; Rumyantsev, V.; Shvarts, M.; Fokanov, V.; Pavlov, A. High current density GaAs and GaSb photovoltaic cells for laser power beaming. In Proceedings of the 3rd World Conference on Photovoltaic Energy Conversion, Osaka, Japan, 11–18 May 2003; Volume 1, pp. 761–764.
17. Peña, R.; Algora, C.; Anton, I. GaAs multiple photovoltaic converters with an efficiency of 45% for monochromatic illumination. In Proceedings of the 3rd World Conference on Photovoltaic Energy Conversion, Osaka, Japan, 11–18 May 2003; pp. 228–231.
18. Kalyuzhnyy, N.A.; Emelyanov, V.M.; Mintairov, S.A.; Shvarts, M.Z. InGaAs metamorphic laser (λ = 1064 nm) power converters with over 44% efficiency. *AIP Conf. Proc.* **2018**, *2012*, 110002. [CrossRef]
19. Kim, Y.; Shin, H.-B.; Lee, W.-H.; Jung, S.H.; Kim, C.Z.; Kim, H.; Lee, Y.T.; Kang, H.K. 1080 nm InGaAs laser power converters grown by MOCVD using InAlGaAs metamorphic buffer layers. *Sol. Energy Mater. Sol. Cells* **2019**, *200*, 109984. [CrossRef]
20. Law, H.D.; Ng, W.W.; Nakano, K.; Dapkus, P.D.; Stone, D.R. High Efficiency InGaAsP Photovoltaic Power Converter. *IEEE Electron Device Lett.* **1981**, *2*, 26–27. [CrossRef]
21. Panchak, A.N.; Pokrovskiy, P.V.; Malevskiy, D.A.; Larionov, V.R.; Shvarts, M.Z. High-Efficiency Conversion of High-Power-Density Laser Radiation. *Tech. Phys. Lett.* **2019**, *45*, 24–26. [CrossRef]
22. Bett, A.W.; Dimroth, F.; Lockenhoff, R.; Oliva, E.; Schubert, J. III–V solar cells under monochromatic illumination. In Proceedings of the 2008 33rd IEEE Photovoltaic Specialists Conference, San Diego, CA, USA, 11–16 May 2008; p. 4922910.
23. Fahrenbruch, A.L.; Lopez-Otero, A.; Werthen, J.G.; Wu, T.C. GaAs- and InAlGaAs-based concentrator-type cells for conversion of power transmitted by optical fibers. In Proceedings of the Conference Record of the Twenty Fifth IEEE Photovoltaic Specialists Conference—1996, Washington, DC, USA, 13–17 May 1996; pp. 117–120.
24. Fave, A.; Kaminski, A.; Gavand, M.; Mayet, L.; Laugier, A. GaAs converter for high power laser diode. In Proceedings of the Conference Record of the Twenty Fifth IEEE Photovoltaic Specialists Conference—1996, Washington, DC, USA, 13–17 May 1996; pp. 101–104.

25. Green, M.; Zhao, J.; Wang, A.; Wenham, S. 45% efficient silicon photovoltaic cell under monochromatic light. *IEEE Electron Device Lett.* **1992**, *13*, 317–318. [CrossRef]

26. Höhn, O.; Walker, A.W.; Bett, A.W.; Helmers, H. Optimal laser wavelength for efficient laser power converter operation over temperature. *Appl. Phys. Lett.* **2016**, *108*, 241104. [CrossRef]

27. Shan, T.; Qi, X. Design and optimization of GaAs photovoltaic converter for laser power beaming. *Infrared Phys. Technol.* **2015**, *71*, 144–150. [CrossRef]

28. Khvostikov, V.P.; Sorokina, S.V.; Potapovich, N.S.; Khvostikova, O.A.; Timoshina, N.K.; Shvarts, M.Z. Modification of Photovoltaic Laser-Power (λ = 808 nm) Converters Grown by LPE. *Semiconductors* **2018**, *52*, 366–370. [CrossRef]

29. Khvostikov, V.P.; Sorokina, S.V.; Potapovich, N.S.; Khvostikova, O.A.; Timoshina, N.K. Laser (λ = 809 nm) power converter based on GaAs. *Semiconductors* **2017**, *51*, 645. [CrossRef]

30. Helmers, H.; Franke, A.; Lackner, D.; Höhn, O.; Predan, F.; Dimroth, F. 51% Efficient Photonic Power Converters for O-Band Wavelengths around 1310 nm. In Proceedings of the 2020 47th IEEE Photovoltaic Specialists Conference (PVSC), Calgary, AB, Canada, 15 June–21 August 2020; pp. 2471–2474, 9300717.

31. Zhao, Y.; Liang, P.; Ren, H.; Han, P. Enhanced efficiency in 808 nm GaAs laser power converters via gradient doping. *AIP Adv.* **2019**, *9*, 105206. [CrossRef]

32. York, M.C.A.; Fafard, S. High efficiency phototransducers based on a novel vertical epitaxial heterostructure architecture (VEHSA) with thin p/n junctions. *J. Phys. D Appl. Phys.* **2017**, *50*, 173003. [CrossRef]

33. Huang, J.; Sun, Y.; Zhao, Y.; Yu, S.; Li, K.; Dong, J.; Xue, J.; Xue, C.; Ye, Y. Characterizations of high-voltage vertically-stacked GaAs laser power converter. *J. Semicond.* **2018**, *39*, 094006. [CrossRef]

34. Ding, Y.; Li, Q.; Lu, Y.; Wang, J. TO-packaged, multi-junction GaAs laser power converter with output electric power over 1 W. In Proceedings of the Conference on Lasers and Electro-Optics Pacific Rim (CLEO-PR), Singapore, 31 July–4 August 2017; pp. 1–3.

35. Jarvis, S.D.; Mukherjee, J.; Perren, M.; Sweeney, S.J. Development and characterisation of laser power converters for optical power transfer applications. *IET Optoelectron.* **2014**, *8*, 64–70. [CrossRef]

36. Khvostikov, V.P.; Sorokina, S.V.; Khvostikova, O.A.; Potapovich, N.S.; Malevskaya, A.V.; Nakhimovich, M.V.; Shvarts, M.Z. GaSb photovoltaic cells for laser power conversion. *AIP Conf. Proc.* **2019**, *2149*, 050007. [CrossRef]

37. Fafard, S.; Masson, D.; Werthen, J.-G.; Liu, J.; Wu, T.-C.; Hundsberger, C.; Schwarzfischer, M.; Steinle, G.; Gaertner, C.; Piemonte, C.; et al. Power and Spectral Range Characteristics for Optical Power Converters. *Energies* **2021**, *14*, 4395. [CrossRef]

38. Keller, G. GaAs multi-junction laser power converters at AZUR SPACE: Current status and development activities. Presented at the 1st Optical Wireless and Fiber Power Transmission Conference 2019, Yokohama, Japan, 23–25 April 2019; pp. 11–12.

39. Wojtczuk, S.J. Long-wavelength laser power converters for optical fibers. In Proceedings of the Conference Record of the Twenty Sixth IEEE Photovoltaic Specialists Conference—1997, Anaheim, CA, USA, 29 September–3 October 1997; pp. 971–974.

40. Eggert, N.; Rusack, R.; Mans, J. Evaluation of photonic power converters. *J. Instrum.* **2010**, *5*, T02001. [CrossRef]

41. Fafard, S.; Masson, D.P. Perspective on photovoltaic optical power converters. *J. Appl. Phys.* **2021**, *130*, 160901. [CrossRef]

42. Wang, A.-C.; Sun, Y.-R.; Yu, S.-Z.; Yin, J.-J.; Zhang, W.; Wang, J.-S.; Fu, Q.-X.; Han, Y.-H.; Qin, J.; Dong, J.-R. Characteristics of 1520 nm InGaAs multijunction laser power converters. *Appl. Phys. Lett.* **2021**, *119*, 243902. [CrossRef]

43. Kurooka, K.; Honda, T.; Komazawa, Y.; Warigaya, R.; Uchida, S. A 46.7% efficient GaInP photonic power converter under high-power 638 nm laser uniform irradiation of 1.5 W cm$^{-2}$. *Appl. Phys. Express* **2022**, *15*, 062003. [CrossRef]

44. Helmers, H.; Hohn, O.; Tibbits, T.; Schauerte, M.; Amin, H.M.N.; Lackner, D. Unlocking 1550 nm laser power conversion by InGaAs single- and multiple-junction PV cells. In Proceedings of the PVSC 2022—IEEE 49th PVSC 2016—IEEE 43rd Photovoltaic Specialists Conference, Philadelphia, PA, USA, 5–10 June 2022.

45. Fafard, S.; Masson, D.P. High-Efficiency and High-Power Multijunction InGaAs/InP Photovoltaic Laser Power Converters for 1470 nm. *Photonics* **2022**, *9*, 438. [CrossRef]

46. Fafard, S.; Masson, D.P. 74.7% Efficient GaAs-based laser power converters at 808 nm at 150 K. *Photonics* **2022**, *9*, 579. [CrossRef]

47. Khvostikov, V.P.; Sorokina, S.V.; Khvostikova, O.A.; Nakhimovich, M.V.; Shvarts, Z. Ge-Based Photovoltaic Laser-Power Converters. *IEEE J. Photovolt.* **2023**, *13*, 254–259. [CrossRef]

48. Gou, Y.; Wang, H.; Wang, J.; Zhang, Y.; Niu, R.; Chen, X.; Wang, B.; Xiao, Y.; Zhang, Z.; Liu, W.; et al. 1064 nm InGaAs metamorphic laser power converts with over 44% efficiency. *Opt. Express* **2022**, *30*, 42178–42185. [CrossRef]

49. Yin, J.; Sun, Y.; Wang, A.; Yu, S.; Wang, J.; Fu, Q.; Qin, J.; Han, Y.; Zhang, W.; Zhang, S.; et al. High-Voltage 1064 nm InGaAsP Multijunction Laser Power Converters. *IEEE Electron Device Lett.* **2022**, *43*, 1291. [CrossRef]

50. Gou, Y.; Wang, H.; Wang, J.; Niu, R.; Chen, X.; Wang, B.; Xiao, Y.; Zhang, Z.; Liu, W.; Yang, H.; et al. High-performance laser power converts for direct-energy applications. *Opt. Express* **2022**, *30*, 31509–31517. [CrossRef]

51. Beattie, M.N.; Helmers, H.; Forcade, G.P.; Valdivia, C.E.; Höhn, O.; Hinzer, K. InP-and GaAs-Based Photonic Power Converters under O-Band Laser Illumination: Performance Analysis and Comparison. *IEEE J. Photovolt.* **2022**, *13*, 113–121. [CrossRef]

52. Fafard, S.; York, M.C.A.; Proulx, F.; Wilkins, M.; Valdivia, C.E.; Bajcsy, M.; Ban, D.; Arès, R.; Aimez, V.; Hinzer, K.; et al. Ultra-efficient N-junction photovoltaic cells with VOC > 14 V at high optical input powers. In Proceedings of the 2016 IEEE 43rd Photovoltaic Specialists Conference (PVSC), Portland, OR, USA, 5–10 June 2016; p. 2374.

53. Wang, A.-C.; Yin, J.-J.; Yu, S.-Z.; Sun, Y.-R.; Dong, J.-R. Origins of the short circuit current of a current mismatched multijunction photovoltaic cell considering subcell reverse breakdown. *Opt. Express* **2023**, *31*, 14482. [CrossRef]

54. Wang, A.-C.; Yin, J.-J.; Yu, S.-Z.; Sun, Y.-R. Multiple tunnel diode peaks in I–V curves of a multijunction laser power converter. *Appl. Phys. Lett.* **2022**, *121*, 233901. [CrossRef]

55. Hartenstein, M.B.; France, R.M.; Nemeth, W.; Theingi, S.; Page, M.; Agarwal, S.; Young, D.L.; Stradins, P. High-voltage monocrystalline Si photovoltaic minimodules based on poly-Si/SiO passivating contacts for high-power laser power conversion. *Sol. Energy Mater. Sol. Cells* **2023**, *255*, 112286. [CrossRef]

56. Ghods, A.; Sandquist, D.; Tatah, K.; Dummer, M.; Xu, G.; Ambrosius, E.; Ren, J.; Johnson, K. Design, fabrication, and characterization of multi-junction micro-photovoltaic devices. In Proceedings of the Physics, Simulation, and Photonic Engineering of Photovoltaic Devices XII, San Francisco, CA, USA, 10 March 2023; Volume 12416, p. 1241607.

57. Chancerel, F.; Regreny, P.; Leclercq, J.L.; Volatier, M.; Jaouad, A.; Darnon, M.; Fafard, S.; Gendry, M.; Aimez, V. Comparison of various InGaAs-based solar cells for concentrated photovoltaics applications. *AIP Conf. Proc.* **2022**, *2550*, 020002.

58. Wang, H.; Wang, J.; Yang, H.; Deng, G.; Yang, Q.; Niu, R.; Gou, Y. The Effect of Non-Uniform Irradiation on Laser Photovoltaics: Experiments and Simulations. *Photonics* **2022**, *9*, 493. [CrossRef]

59. Khvostikov, V.P.; Panchak, A.N.; Khvostikova, O.A.; Pokrovskiy, P.V. Side-Input GaAs Laser Power Converters with Gradient AlGaAs Waveguide. *IEEE Electron Device Lett.* **2022**, *43*, 1717–1719. [CrossRef]

60. Ding, G.; Zheng, Y.; Li, Q.; Zhang, G.; Guo, X.; Wang, H.; Xiao, X.; Feng, Y.; Bai, Y.; Shao, Y. Constructing microcavity for perovskite laser power converter: A theoretical study. *Phys. Status Solidi (A)* **2022**, *219*, 2200539. [CrossRef]

61. Lozano, J.F.; Seoane, N.; Almonacid, F.; Fernández, E.F.; García-Loureiro, A. Laser Power Converter Architectures Based on 3C-SiC with Efficiencies > 80%. *Sol. RRL* **2022**, *6*, 2101077. [CrossRef]

62. Fernández, E.F.; García-Loureiro, A.; Seoane, N.; Almonacid, F. Band-gap material selection for remote high-power laser transmission. *Sol. Energy Mat. Sol. Cells* **2022**, *235*, 111483. [CrossRef]

63. France, R.M.; Buencuerpo, J.; Bradsby, M.; Geisz, J.F.; Sun, Y.; Dhingra, P.; Lee, M.L.; Steiner, M.A. Graded buffer Bragg reflectors with high reflectivity and transparency for metamorphic optoelectronics. *J. Appl. Phys.* **2021**, *129*, 173102. [CrossRef]

64. Beattie, M.N.; Valdivia, C.E.; Wilkins, M.M.; Zamiri, M.; Kaller, K.L.C.; Tam, M.C.; Kim, H.S.; Krich, J.J.; Wasilewski, Z.R.; Hinzer, K. High current density tunnel diodes for multi-junction photovoltaic devices on InP substrates. *Appl. Phys. Lett.* **2021**, *118*, 062101. [CrossRef]

65. Wagner, L.; Reichmuth, S.K.; Philipps, S.P.; Oliva, E.; Bett, A.W.; Helmers, H. Integrated series/parallel connection for photovoltaic laser power converters with optimized current matching. *Prog. Photovolt. Res. Appl.* **2020**, *29*, 172. [CrossRef]

66. Panchak, A.; Khvostikov, V.; Pokrovskiy, P. AlGaAs gradient waveguides for vertical p/n junction GaAs laser power converters. *Opt. Laser Technol.* **2021**, *136*, 106735. [CrossRef]

67. Lin, M.; Sha, W.E.I.; Zhong, W.; Xu, D. Intrinsic losses in photovoltaic laser power converters. *Appl. Phys. Lett.* **2021**, *118*, 104103. [CrossRef]

68. Zhao, Y.; Li, S.; Ren, H.; Li, S.; Han, P. Energy band adjustment of 808 nm GaAs laser power converters via gradient doping. *J. Semicond.* **2021**, *42*, 032701. [CrossRef]

69. Nouri, N.; Valdivia, C.E.; Beattie, M.N.; Zamiri, M.S.; Krich, J.J.; Hinzer, K. Ultrathin monochromatic photonic power converters with nanostructured back mirror for light trapping of 1310-nm laser illumination. In Proceedings of the Physics, Simulation, and Photonic Engineering of Photovoltaic Devices X, Online, 5 March 2021; Volume 11681, p. 116810X.

70. Masson, D.; Proulx, F.; Fafard, S. Pushing the limits of concentrated photovoltaic solar cell tunnel junctions in novel high-efficiency GaAs phototransducers based on a vertical epitaxial heterostructure architecture. *Prog. Photovolt. Res. Appl.* **2015**, *23*, 1687–1696. [CrossRef]

71. Fafard, S.; Masson, D.P. Transducer to Convert Optical Energy to Electrical Energy. U.S. Patent 9,673,343, 6 June 2017.

72. Wulf, J.; Oliva, E.; Mikolasch, G.; Bartsch, J.; Dimroth, F.; Helmers, H. Thin film GaAs solar cell enabled by direct rear side plating and patterned epitaxial lift-off. In Proceedings of the 2021 IEEE 48th Photovoltaic Specialists Conference (PVSC), Fort Lauderdale, FL, USA, 20–25 June 2021.

73. Helmers, H.; Lopez, E.; Hohn, O.; Lackner, D.; Schon, J.; Schauerte, M.; Schachtner, M.; Dimroth, F.; Bett, A.W. Pushing the Boundaries of Photovoltaic Light to Electricity Conversion: A GaAs Based Photonic Power Converter with 68.9% Efficiency. In Proceedings of the 2021 IEEE 48th Photovoltaic Specialists Conference (PVSC), Fort Lauderdale, FL, USA, 20–25 June 2021; pp. 2286–2289.

74. Schauerte, M.; Hohn, O.; Wierzkowski, T.; Keller, G.; Helmers, H. 4-Junction GaAs Based Thin Film Photonic Power Converter with Back Surface Reflector for Medical Applications. In Proceedings of the 2021 IEEE 48th Photovoltaic Specialists Conference (PVSC), Fort Lauderdale, FL, USA, 20–25 June 2021; pp. 1954–1959.

75. France, R.M.; Hinojosa, M.; Ahrenkiel, S.P.; Young, M.R.; Johnston, S.W.; Guthrey, H.L.; Steiner, M.A.; Geisz, J.F. Improvement of front-junction GaInP by point-defect injection and annealing. In Proceedings of the 2021 IEEE 48th Photovoltaic Specialists Conference (PVSC), Fort Lauderdale, FL, USA, 20–25 June 2021; p. 2522.

76. Geisz, J.F.; Buencuerpo, J.; McMahon, W.E.; Klein, T.R.; Tamboli, A.C.; Warren, E.L. Fabrication, Measurement, and Modeling of GaInP/GaAs Three-Terminal Cells and Strings. In Proceedings of the 2021 IEEE 48th Photovoltaic Specialists Conference (PVSC), Fort Lauderdale, FL, USA, 20–25 June 2021; pp. 0154–0157.

77. Yamaguchi, M.; Dimroth, F.; Geisz, J.F.; Ekins-Daukes, N.J. Multi-junction solar cells paving the way for super high-efficiency. *J. Appl. Phys.* **2021**, *129*, 240901. [CrossRef]

78. Kimovec, R.; Helmers, H.; Bett, A.W.; Topič, M. Comprehensive electrical loss analysis of monolithic interconnected multi-segment laser power converters. *Prog. Photovolt. Res. Appl.* **2019**, *27*, 199. [CrossRef]
79. Kimovec, R.; Helmers, H.; Bett, A.W.; Topic, M. On the Influence of the Photo-Induced Leakage Current in Monolithically Interconnected Modules. *IEEE J. Photovolt.* **2018**, *8*, 541–546. [CrossRef]
80. Cicic, S.; Tomic, S. Automated design of multi junction solar cells by genetic approach: Reaching the >50% efficiency target. *Sol. Energy Mater. Sol. Cells* **2018**, *181*, 30–37. [CrossRef]
81. Čičić, S.; Tomić, S. Genetic algorithm designed high efficiency laser power converters based on the vertical epitaxial heterostructure architecture. *Sol. Energy Mater. Sol. Cells* **2019**, *200*, 109878. [CrossRef]
82. CAlgora; García, I.; Delgado, M.; Peña, R.; Vázquez, C.; Hinojosa, M.; Rey-Stolle, I. Beaming power: Photovoltaic laser power converters for power-by-light. *Joule* **2022**, *6*, 340. [CrossRef]
83. Kalyuzhnyy, N.A.; Emelyanov, V.M.; Evstropov, V.V.; Mintairov, S.A.; Mintairov, M.A.; Nahimovich, M.V.; Salii, R.A.; Shvarts, M.Z. Optimization of photoelectric parameters of InGaAs metamorphic laser ($\lambda$ = 1064 nm) power converters with over 50% efficiency. *Sol. Energy Mater. Sol. Cells* **2020**, *217*, 110710. [CrossRef]
84. Proulx, F.; York, M.C.A.; Provost, P.O.; Arès, R.; Aimez, V.; Masson, D.P.; Fafard, S. Measurement of strong photon recycling in ultra-thin GaAs n/p junctions monolithically integrated in high-photovoltage vertical epitaxial heterostructure architectures with conversion efficiencies exceeding 60%. *Phys. Status Solidi RRL* **2017**, *11*, 1600385. [CrossRef]
85. Wilkins, M.; Valdivia, C.E.; Gabr, A.M.; Masson, D.; Fafard, S.; Hinzer, K. Luminescent coupling in planar opto-electronic de-vices. *J. Appl. Phys.* **2015**, *118*, 143102. [CrossRef]
86. Lopez, E.; Höhn, O.; Schauerte, M.; Lackner, D.; Schachtner, M.; Reichmuth, S.K.; Helmers, H. Experimental coupling process efficiency and benefits of back surface reflectors in photovoltaic multi-junction photonic power converters. *Prog. Photovolt. Res. Appl.* **2021**, *29*, 461. [CrossRef]
87. Xia, D.; Krich, J.J. Efficiency increase in multijunction monochromatic photovoltaic devices due to luminescent coupling. *J. Appl. Phys.* **2020**, *128*, 013101. [CrossRef]
88. Philipps, S.P.; Hoheisel, R.; Gandy, T.; Stetter, D.; Hermle, M.; Dimroth, F.; Bett, A.W. An experimental and theoretical study on the temperature dependence of GaAs solar cells. In Proceedings of the 2011 37th IEEE Photovoltaic Specialists Conference, Seattle, WA, USA, 19–24 June 2011; pp. 001610–001614.
89. Putra, E.P.; Theivindran, R.; Hasnul, H.; Lee, H.J.; Ker, P.J.; Jamaludin, M.Z.; Awang, R.; Mohd Yusof, F.A. Technology up-date on patent and development trend of power over fiber: A critical review and future prospects. *J. Photonics Energy* **2023**, *13*, 011001. [CrossRef]
90. Guo, C.; Guan, C.; Lv, H.; Chai, S.; Chen, H. Multi-Channel Long-Distance Audio Transmission System Using Power-over-Fiber Technology. *Photonics* **2023**, *10*, 521. [CrossRef]
91. Martinek, P.; Prajzler, V. Power over fiber using a large core fiber and laser operating at 976 nm with 10 W power. *Opt. Fiber Technol.* **2023**, *80*, 103404. [CrossRef]
92. Shindo, N.; Kobatake, T.; Masson, D.; Fafard, S.; Matsuura, M. Optically Powered and Controlled Drones Using Optical Fibers for Airborne Base Stations. *Photonics* **2022**, *9*, 882. [CrossRef]
93. Matsuura, M.; Nomoto, H.; Mamiya, H.; Higuchi, T.; Masson, D.; Fafard, S. Over 40-W Electric Power and Optical Data Transmission Using an Optical Fiber. *IEEE Trans. Power Electron.* **2020**, *36*, 4532. [CrossRef]
94. Helmers, H.; Armbruster, C.; von Ravenstein, M.; Derix, D.; Schoner, C. 6-W Optical Power Link with Integrated Optical Data Transmission. *IEEE Trans. Power Electron.* **2020**, *35*, 7904. [CrossRef]
95. Jaffe, P.; Jenkins, P.; US NRL; Nugent, T.; PowerLight Tech. Inc. Practical Power Beaming Gets Real, IEEE Spectrum 21 May 2022. 2019. Available online: https://spectrum.ieee.org/power-beaming (accessed on 14 July 2023).
96. Wilkins, M.M.; Ishigaki, M.; Provost, P.-O.; Masson, D.; Fafard, S.; Valdivia, C.E.; DeDe, E.M.; Hinzer, K. Ripple-Free Boost-Mode Power Supply Using Photonic Power Conversion. *IEEE Trans. Power Electron.* **2018**, *34*, 1054. [CrossRef]
97. Sweeney, S.J. Optical wireless power at eye-safe wavelengths: Challenges and opportunities. In Proceedings of the 3rd Optical Wireless and Fiber Power Transmission Conference (OWPT2021), Yokohama, Japan, 19–22 April 2021.
98. Wong, Y.L.; Shibui, S.; Koga, M.; Hayashi, S.; Uchida, S. Optical Wireless Power Transmission Using a GaInP Power Converter Cell under High-Power 635 nm Laser Irradiation of 53.5 W/cm$^2$. *Energies* **2022**, *15*, 3690. [CrossRef]
99. He, T.; Yang, S.-H.; Zhang, H.-Y.; Zhao, C.-M.; Zhang, Y.-C.; Xu, P.; Muñoz, M. High-Power High-Efficiency Laser Power Transmission at 100 m Using Optimized Multi-Cell GaAs Converter. *Chin. Phys. Lett.* **2014**, *31*, 104203. [CrossRef]
100. Khvostikov, V.P.; Kalyuzhnyy, N.A.; Mintairov, S.A.; Potapovich, N.S.; Sorokina, S.V.; Shvarts, M.Z. Module of Laser-Radiation ($\lambda$ = 1064 nm) Photovoltaic Converters. *Semiconductors* **2019**, *53*, 1110–1113. [CrossRef]
101. Guan, C.; Li, L.; Ji, H.; Luo, S.; Xu, P.; Gao, Q.; Lv, H.; Liu, W. Fabrication and Characterization of a High-Power Assembly with a 20-Junction Monolithically Stacked Laser Power Converter. *IEEE J. Photovolt.* **2018**, *8*, 1355–1362. [CrossRef]